HISTO-MRI

HISTO-MRI Project

This project has received funding from the European Union's H2020 Programme under grant agreement no 737180— HISTO-MRI

D2.2: Report on the Simulations Results for Magnet and RF coil

Participants Deliverable:
1. – Agencia Estatal Consejo Superior de Investigaciones Científicas (CSIC).
2. – Tesoro Imaging S.L.
3. – Leiden University Medical Center (LUMC).

Version	Date	Reviewer
1	19/12/2017	Juan Pablo Rigla/Tesoro Imaging S.L.
2A	28/12/2017	Elena Díaz Caballero / Tesoro Imaging S.L.
3A	3/01/2018	José Miguel Algarín Guisado / CSIC
2B	7/01/2018	Andrew Webb / LUMC
4	8/01/2018	Elena Díaz Caballero / Tesoro Imaging S.L.
5	26/02/2018	Juan Pablo Rigla Pérez/ Tesoro Imaging S.L.

Table of contents

1 Deliverable description

This deliverable describes the designs and simulations of the magnet system, gradient coils and RF coil designed for the purpose of this project.

This deliverable is the first result of *Tasks 1, 2* and *3, Development of the magnetic system: low magnetic field and pre-polarized magnetic field, Development of the gradient coils,* and *Development of the radiofrequency coils*, respectively, part of **WP2 – Magnetic system, Gradient and RF Coils.**

2 Introduction

The HISTO-MRI system will incorporate an innovative approach with the development of a novel high-field pre-polarized MRI (pMRI) magnet. This MRI scanner will employ two separate fields produced by two different magnets. A pulsed, strong and inhomogeneous magnetic field (up to 20T) will be used to polarize the sample prior to imaging, in order to increase signal-to-noise ratio (SNR) in subsequent evolution images obtained at lower magnetic field strength (1T). At the time of this deliverable, just the design for the low magnetic field magnet can be shown. Preliminary results for the design of the ultra-fast gradient coils are also detailed. The RF system will incorporate a transmit/receive coil and the adequate tuning/matching circuit.

2.1 Main Magnet System

A conceptual design has been made for the low magnetic field electromagnetic dipole with the specifications given in Table 1. The magnet has been designed with circular pole and circular coils and with a so-called H-type of iron yoke, as shown in Fig.1.

Table 1: Low magnetic field magnet specifications.

Pole gap	70 mm
Field of view diameter	20 mm
Field homogeneity	<100 ppm
Maximum Magnetic field	1.0 T

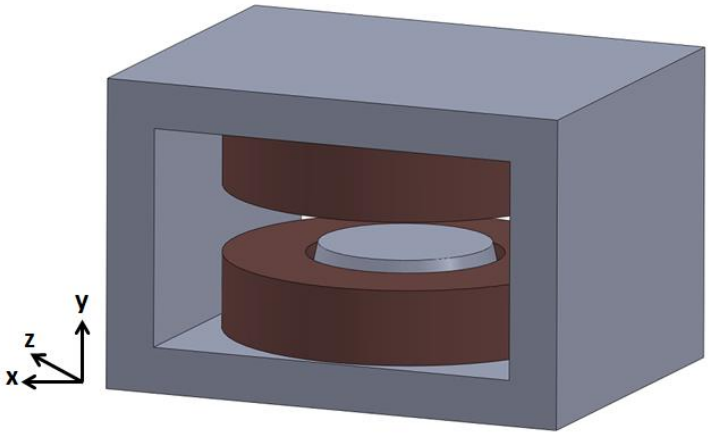

Figure 1: 3D model of the magnet and coordinate system.

With a flat pole profile, the diameter of the pole has been chosen to 250 mm in order to have nominal field homogeneity below the required ±40ppm in the 3D design calculation. For the original larger magnet, we did consider using a special rose-shim to reduce the magnet

size but for this smaller magnet, this is not an attractive concept, as it seems more important to have a flat pole profile to minimize the effects of mechanical imperfections in the pole production.

The magnetic field distribution in the XZ-plane obtained in the simulations con COMSOL is shown in Fig.2. The magnetic field profiles for the Z and X axis are shown in Fig.3. Figure 4 shows the magnetic field distribution, which derives the magnetic saturation of the magnet.

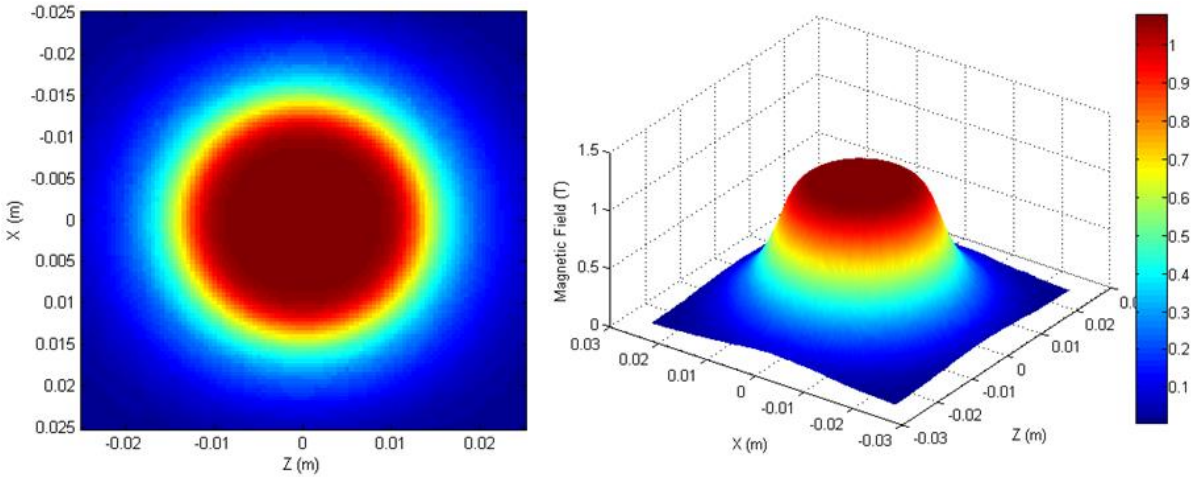

Figure 2: 2D and 3D Magnetic Field distribution in the XZ-plane (y=0) of the electromagnet.

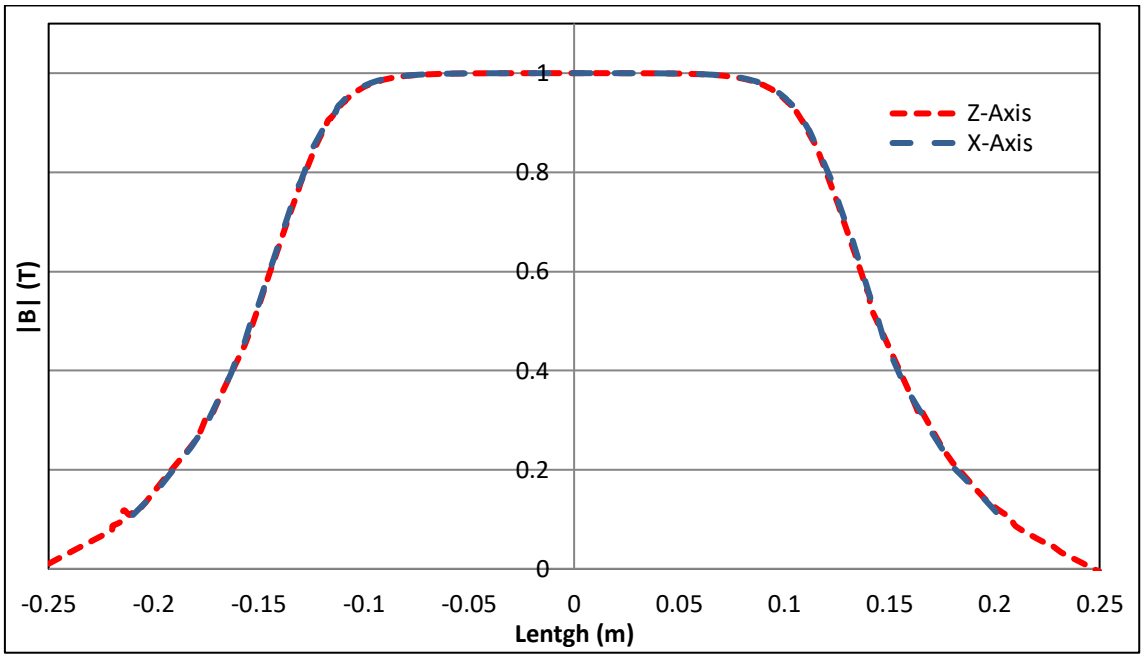

Figure 3: Profile of the magnetic field, |B (T)|, in the median plane along of the Z-axis and X-Axis.

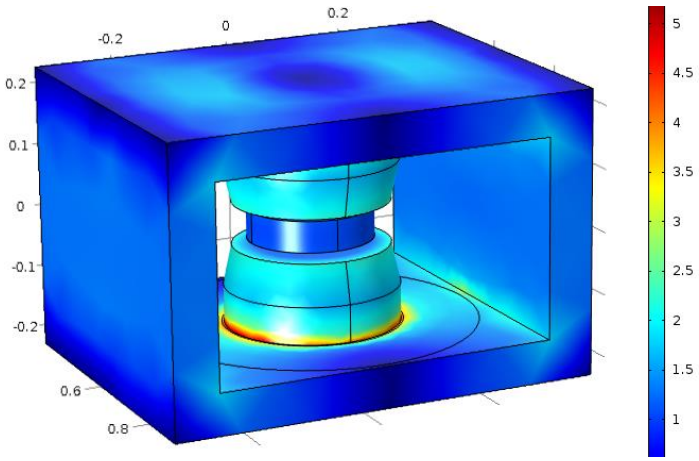

Figure 4: 3D Magnetic Field distribution.

With this 250 mm wide pole the calculated field homogeneity is within the specified ±40 ppm, as shown in Fig.5. The homogeneity is evaluated on radius 10mm circles in respectively the XZ, YZ and XY plane. The pole profile has to be produced to tight mechanical tolerances in order to avoid a significant degradation of the field homogeneity. With allowed mechanical pole gap error of dG=0.02mm the relative gap error is now dG/G = 0.02/70 = 286 ppm. If the pole surface is perfectly flat then a 0.02 mm gap error in the full pole width will only result in a minimal field error within the 10 mm good field radius. A relative field inhomogeneity error contribution of for example maximum 30 ppm will, however, require a 0.002 mm local pole gap uniformity.

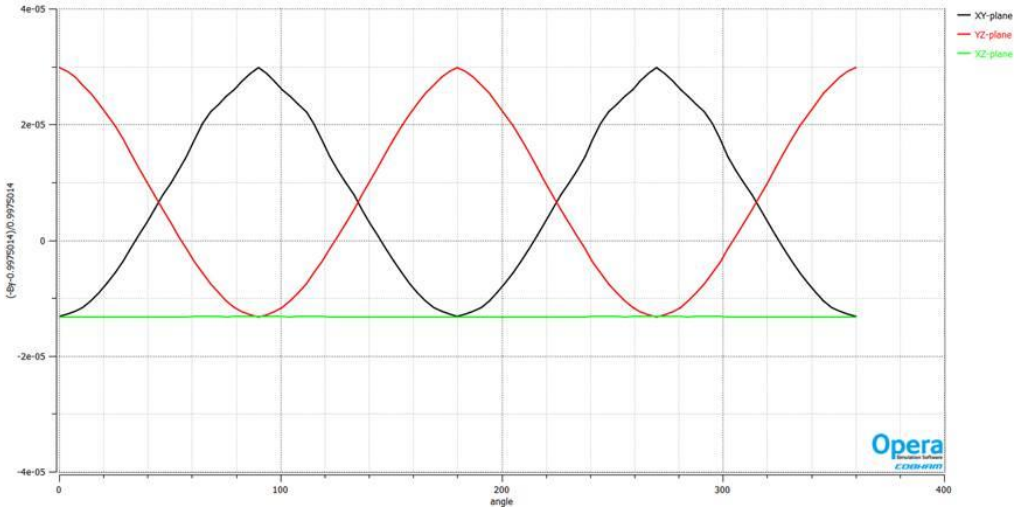

Figure 5: Field homogeneity calculated from the 3D model at the nominal 1T center field.

The magnet has an iron length of 400 mm, height 500 mm and width 730 mm in the preliminary design. The coils increased the total magnet length to 530 mm. The weight of the model magnet is about 1 Ton. The conceptual coil design requires a nominal current of 183 A to reach a 1T center field. The coils consume up to 5 kW which is to be water cooled. With water pressure of 4 bar, this requires a water flow of about 7.3 L/min for the coil design. The magnet is expected to be ramped from zero to 1T with a ramping time on the order of 30s and operated essentially as a DC type of magnet.

To comply with the international safety regulations regarding the installation of MRI Systems, it is necessary to determine the position of the 5 Gauss line outside the MRI system.

In the simulations it was determined that this line was located at 40cm from the front and back of the magnet. Different alternatives were studied to change the position of the 5 G line.

The optimization process of the magnet is shown below. The length of the yoke was increased from 200 to 270mm and the yoke thickness was reduced from the 90mm to 67mm. To reduce the magnetic field outside the magnet, two steel plates with a thickness of 10mm were installed at distance of 20mm in front and back of the magnet. The mirror plate will have an access hole with dimensions of 72x240mm to allow the access of the samples inside the magnet. 3D CAD magnet with shield steel plates is shown in Fig.6. The magnetic field distribution outside the optimized magnet structure shutout and with the steel plates is shown in Fig.7. The dimensions and weight of the magnet including the shielding system are 594x452x540mm^3 and 907kg, respectively.

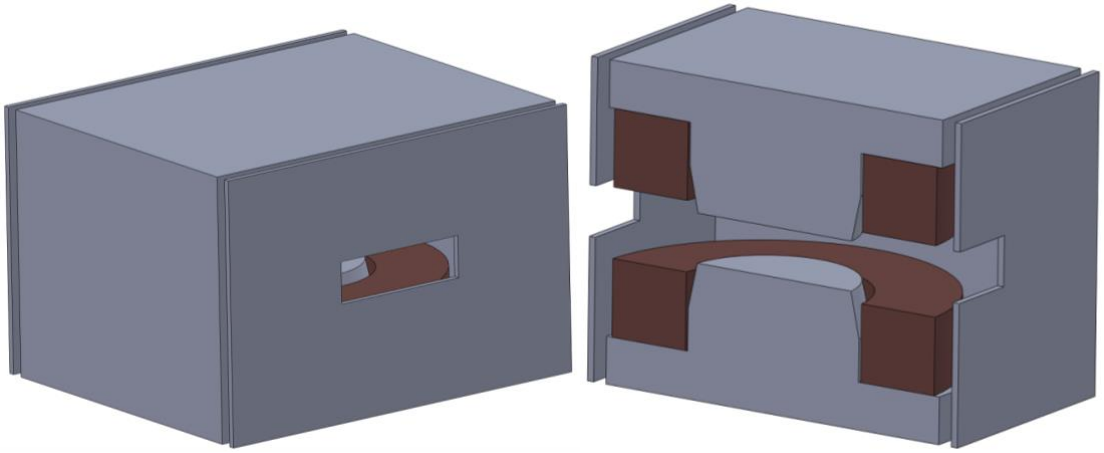

Figure 6: 3D CAD magnet with shield steel plates.

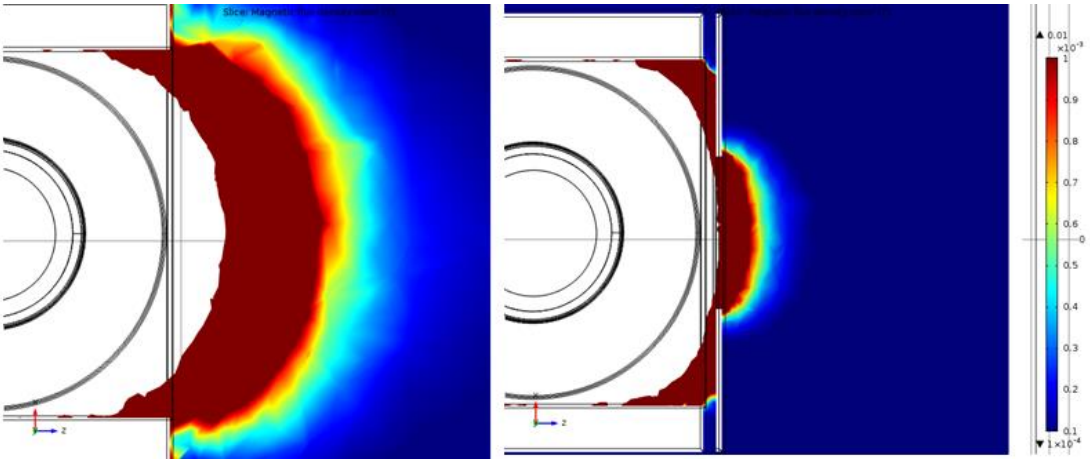

Figure 7: Fringe field distribution in front the magnet face without (left) and with (right) shield steel plates.

2.2 Pre-Polarization Magnetic System

The magnetic pre-polarization system is used to increase the SNR value in MRI systems. This system is formed by a pulsed magnet, which generates a strong magnetic field (B_{pre}>5T/s) orthogonal to the main magnetic field. Unlike the main magnetic field which has to be as homogeneous as possible, the magnetic field generated by the pre-polarizing magnet does not need a high homogeneity. The pulse duration of the pre-polarizing magnetic field must be greater than T_1 and T_2.

For the design of the pre-polarization system, different configurations were studied: Helmholtz coils, solenoid coil… In this study we concluded that the most optimal configuration was a solenoid magnet, because with this configuration is possible to obtain strong magnetic fields. The sample will be placed inside the solenoid. An image of the magnet proposed for the pre-polarization magnetic system is shown in Fig.8. It is a 4-layer solenoid with 33 turns. In this design we obtain an inductance value of 0.046 mH. To reduce the resistance of the solenoid, a wire with a rectangular section (10mm^2) was chosen. We obtain a resistance value of 4.53 mΩ.

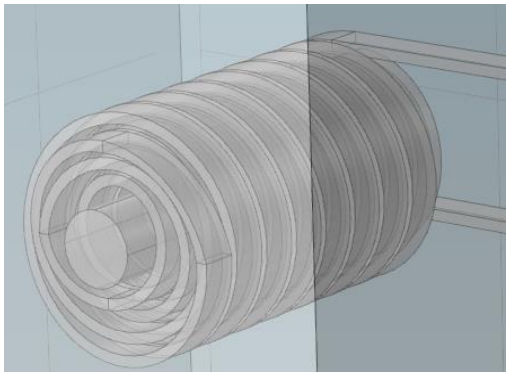

Figure 8: 3D CAD Pre-Polarization magnet.

The optimization of the solenoid geometry and the magnetic study were carried out by means of electromagnetic simulation software. The simulations were performed assuming continuous magnetic field. Figure 9 shows the magnetic profiles along the Z-axis for different current values.

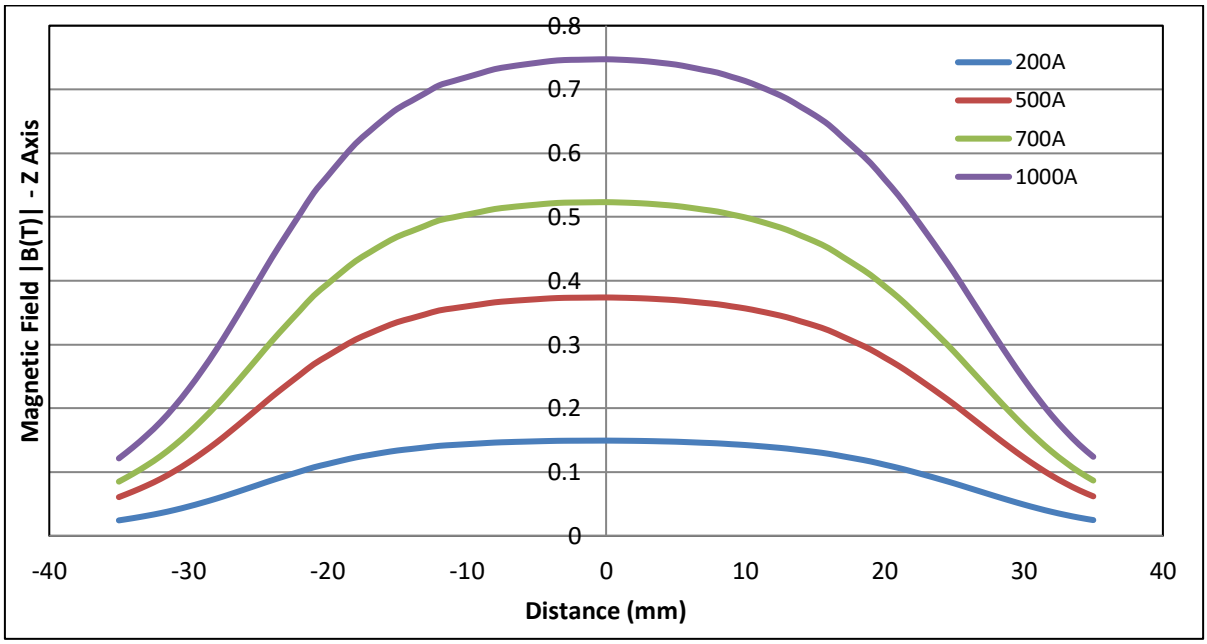

Figure 9: Magnetic field, |B (T)|, profile in the median plane along of the Z-axis (X,Y=0) for different currents.

The thermal behavior of the solenoid was studied due to the high currents (100 [A]) used to generate the magnetic field. As it is a pulsed magnet, the thermal study was performed as a function of time for different pulsed sequences. Figures 10 and 11 shows two of these pulses sequences. Figure 10 shows a pulse sequence where the pulse time (T_{pulse}) is

100ms and the delay time (T_{delay}) between pulses is 400ms. In this case, after one minute of work, the maximum temperature reached in the magnet is 297K. In this case, 8T/s maximum magnetic field value would be reached.

However, in Figure 11 different results are obtained. For this case, the pulse time (T_{pulse}) is 300ms and the delay time (T_{delay}) is 200ms. For this case, temperatures of 3000k and a maximum magnetic field value of 2.66 T / s were obtained.

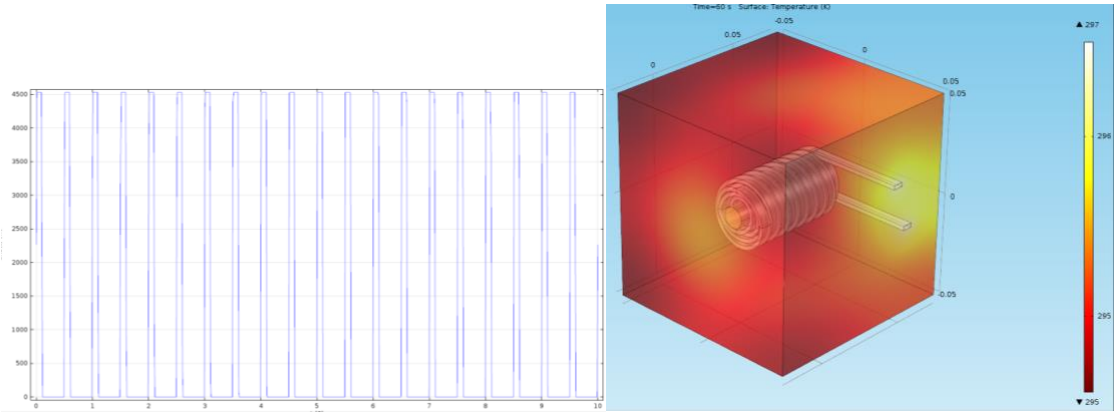

Figure 10: Pre-Polarization Sequence Tpulse=100ms and Tdelay=400ms.

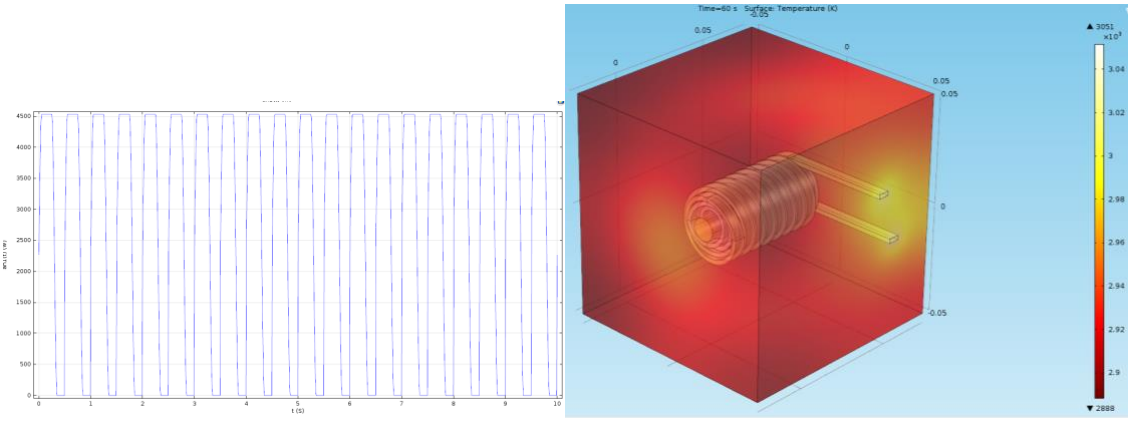

Figure 11: Pre-Polarization Sequence Tpulse=300ms and Tdelay=200ms.

Implementing a cooling system based on LN_2 to ensure proper operation of the pre-polarization system and to ensure that the heat generated by the solenoid can affect the rest of the components of the system and the samples under study also to ensure that the heat generated by the solenoid can affect the rest of the MRI components of the system and the samples under study.

2.3. Gradient Coil

Gradient coil are a main part of a MRI system. The aim of gradient coils is to encode spatially the FoV. Different gradient coil design methods have been presented years ago. Some factors such as linearity, inductance and resistances must be taken into account to obtain an optimized design for the gradient coils.

According to the distance between poles (dPoles) and FoV size, a gradient coil system has been designed. Distance from Y, Z and X gradient coil to center of FoV is 27, 19 and 15 mm,

respectively. Figure 12 shows a preliminary MRI system scheme with all components and their distances.

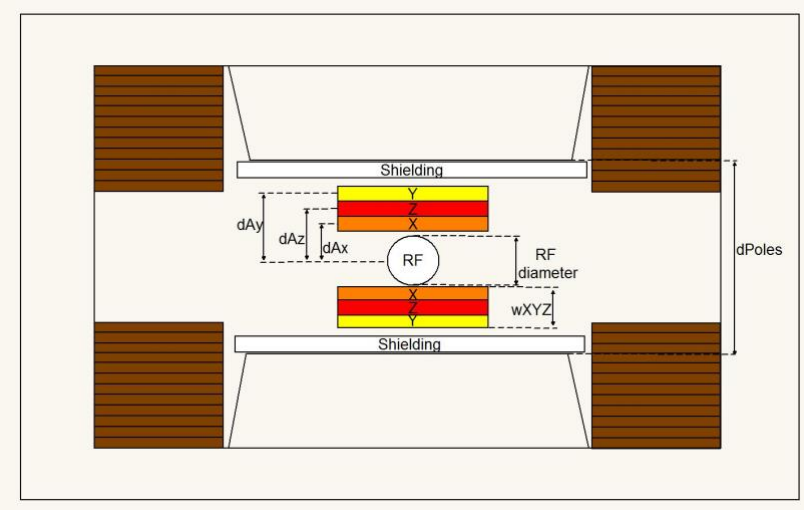

Figure 12: Preliminary MRI system.

In order to get an ultra-fast gradient system, the gradient coils must have both low resistance and inductance. According to that, our study has paid special attention to minimize both the coil length and surface and also to reduce the number of turns.

In this project, the largest area needed to manufacture each gradient is 120x120 mm. Table 2 shows the geometrical and physical gradient coil parameters to obtain a strength field of G=1.2T/m. Simulated gradient field profiles along line Z=0 are shown in Figure 13.

Table 2: Physical and geometrical gradient coil parameters.

	X	**Y**	**Z**
Distance A (mm)	27	19	15
maximum area (mm^2)	115	90	120
g (mT/m/A)/coil	1,4	2,06	1,42
R (mΩ)/coil	3,8	2,3	3,36
L(μH) /coil	5,2	4,1	6
I(A) to G=1,2T/m	425	295	425

Planar gradient coils have been chosen as topology substrate. Simulations suggest that cooling will be necessary. Therefore, in order to refrigerate the heat power generated by gradient coils, copper hollow tube has been selected for manufacturing our coils. The total gradient coil width is 20mm. Simulations suggest that a shielding sheet will be necessary, so a 5mm free gap has been maintained for this purpose as is shown in Figure 12.

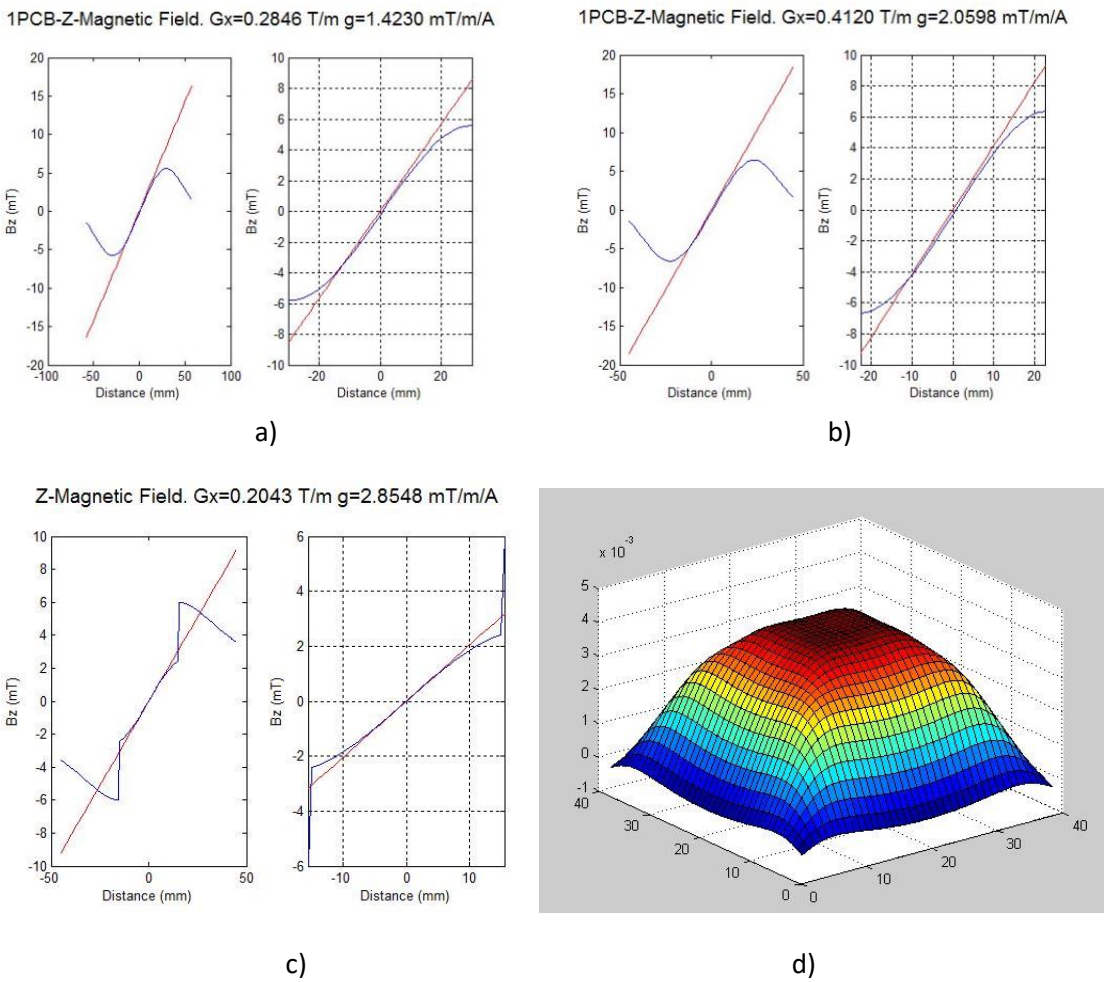

Figure 13: Gradient field obtained for the a) X, b) Y and c) Z gradient coil. d) Magnetic field obtained on the FoV center plane by using the Z-gradient coil.

2.4 RF Coil

Since the rest of the system -including gradient coils, their position, the shielding, etc.- needs to be exactly defined at their definitive implementation in order to define the final RF coil, several options have been designed and simulated in order to be able to fit in the final system.

Two different geometry topologies have been designed and simulated: the solenoid coil and the saddle coil. Figure 14 shows a sketch of both the solenoid and the saddle coil used in CST simulations. Both topologies will be fabricated and tested for the best behaviour. Initially, the dimensions of the RF coil were have a diameter of 30 mm and a length of 45 mm, approximately. A 10 turns solenoid provides higher SNR, sensitivity and Q than the saddle coil, while the saddle coil minimizes the conservative electric field produced by the required tuning capacitors and provides a greater accessibility for the sample. These dimensions provide a good trade-off between sensitivity and homogeneity of the transmitted magnetic field. However, another geometry dimensions have been designed in order to be able to fit the in the final available space between gradient coils (since it seems the separation between them is

going to be narrower than initially expected), and also to have a higher homogeneity in a smaller FOV. In order to do so, 15mm-diameter and 45mm-length 20 turns solenoid and saddle coils have been respectively designed and simulated.

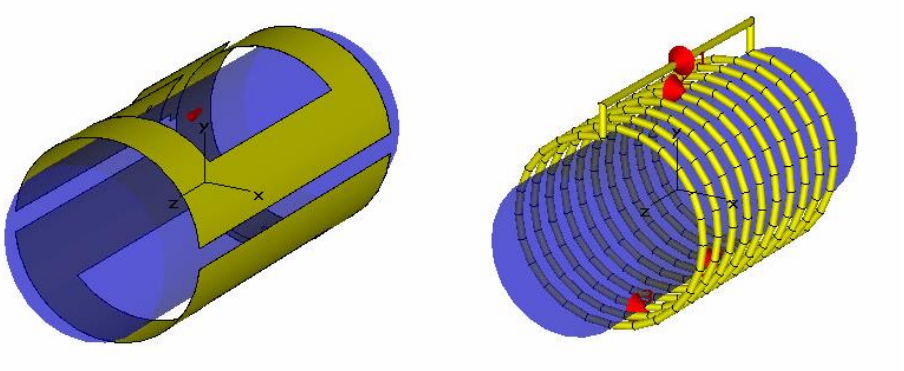

Figure 14. Sketch of the RF coil geometries used in the simulations: single-turn saddle coil (left) and multi-turn solenoid coil (right) simulated. In simulations, the static B0 field points in X direction.

CST simulations have shown that each of the RF coil configurations can be readily impedance matched to 50 Ohms with reasonable values (10-500 pF) of non-magnetic capacitors. A balanced capacitive tune and match circuit has been designed for every coil design. In order to do so, two options are presented for each design. On the one hand, a traditional tuning/matching circuit consisting of fixed and trimmer capacitors. On the other hand, an impedance matching circuit incorporating varactor diodes in order to allow a remote tuning/matching. Figure 15 shows the impedance matching circuit using varactors. Each block (tuning and matching) includes a fixed capacitor and a varactor. They also include DC block capacitors to prevent the DC current flows through the RF coil, as well as DC feeds to filter any AC signal flowing to the DC power supplier.

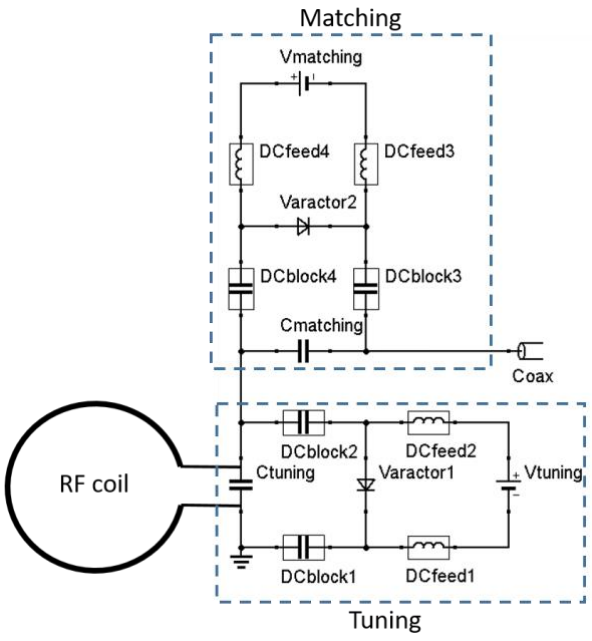

Figure 15. Impedance matching circuit with varactor diodes to allow remote tuning/matching.

The four RF coil designs resonate at a frequency of 42.6 MHz (corresponding to 1 Tesla). The table below shows the most relevant geometrical and simulated parameters for each designed coil:

Table 3:. Geometrical and simulated parameters for each designed coil.

Probe geometry	Saddle	Saddle	Solenoid	Solenoid
Coil diameter	30 mm	15 mm	30 mm	15 mm
Coil length	45 mm	45 mm	45 mm	45 mm
Number of turns	n/a	n/a	10	20
Copper thickness	35µm	35µm	n/a	n/a
Wire diameter	n/a	n/a	1.25mm	1.25mm
Resonant frequency	42.6 MHz	42.6 MHz	42.6 MHz	42.6 MHz
Q value	39	95	52	121
SNR (arbitrary units)	80	180	112	320
B1 (A/m)*	80	180	112	320
Max SAR 10g (W/kg)**	0.11	n/n	0.12	n/n
Max SAR 1g (W/kg)**	n/a	0.22	n/a	0.06

*B1 calculated with an input power of 1 Watt.

**We assume an average input power of 1 Watt with repetition time 10 ms and excitation time 0.1 ms.

n/n = value not necessary to be calculated, n/a = value does not apply to this case.

Figure 16 shows the magnetic field plots on the YZ plane for saddle and solenoid coils with 30 mm diameter. They are matched to 50Ω and the input power is 1 Watt. Both RF coils generate a relatively homogeneous B1 field around the center of the probe. Saddle coil produces the magnetic field along the Y direction while the solenoid produces the magnetic field along the Z direction, both of them orthogonal to the static B0 magnetic field. Beside the magnetic field direction, the plots also show that solenoid coil produces a magnetic field with a higher magnitude than the saddle coil. This implies that excitation field while transmission, as well as sensitivity and SNR while reception, will be higher in solenoid coil than in saddle coil. Simulations show analogous results for saddle and solenoid coils with 15 mm diameter, respectively, but the magnetic field is higher in magnitude due to the smaller size. Therefore, the RF coils with 15 mm will provide better image quality but in a smaller field of view.

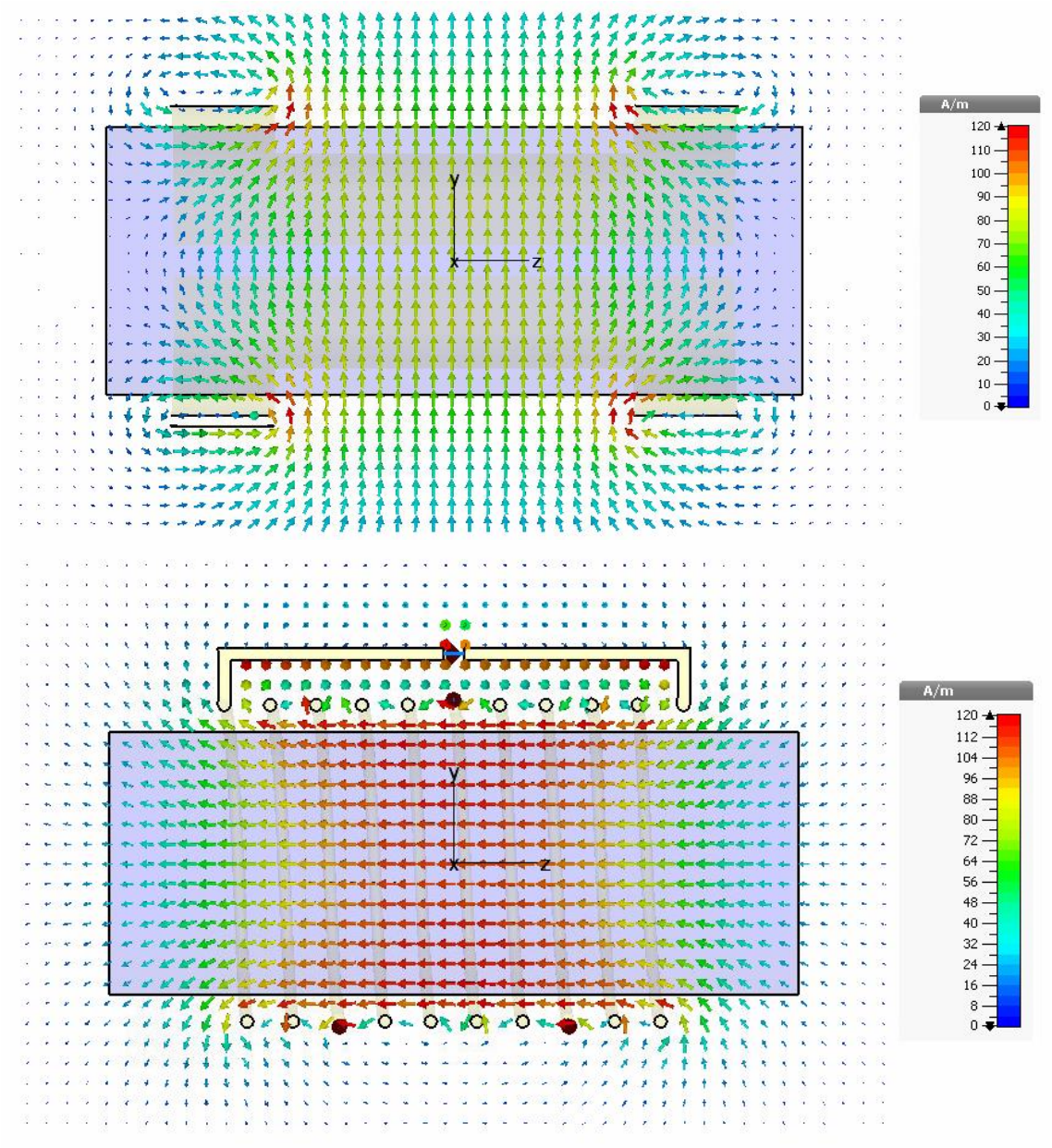

Figure 16. Magnetic field plots on the YZ plane for saddle coil (top) and solenoid coil (bottom) with 30 mm diameter.

The Figure 17 shows the magnetic field deviation in % along the different axis for the designed and simulated coils. The results show that magnetic field produced by the solenoid coil is more homogeneous for both diameters, 30 mm and 15 mm. For 30 mm diameter, numerical calculations show that, in XY plane, a 90% of the inner area has a magnetic field deviation smaller than 5% for solenoid coil, while this area is only 50% for the saddle coil. Numerical simulations for RF coils with 15 mm diameter provided similar results.

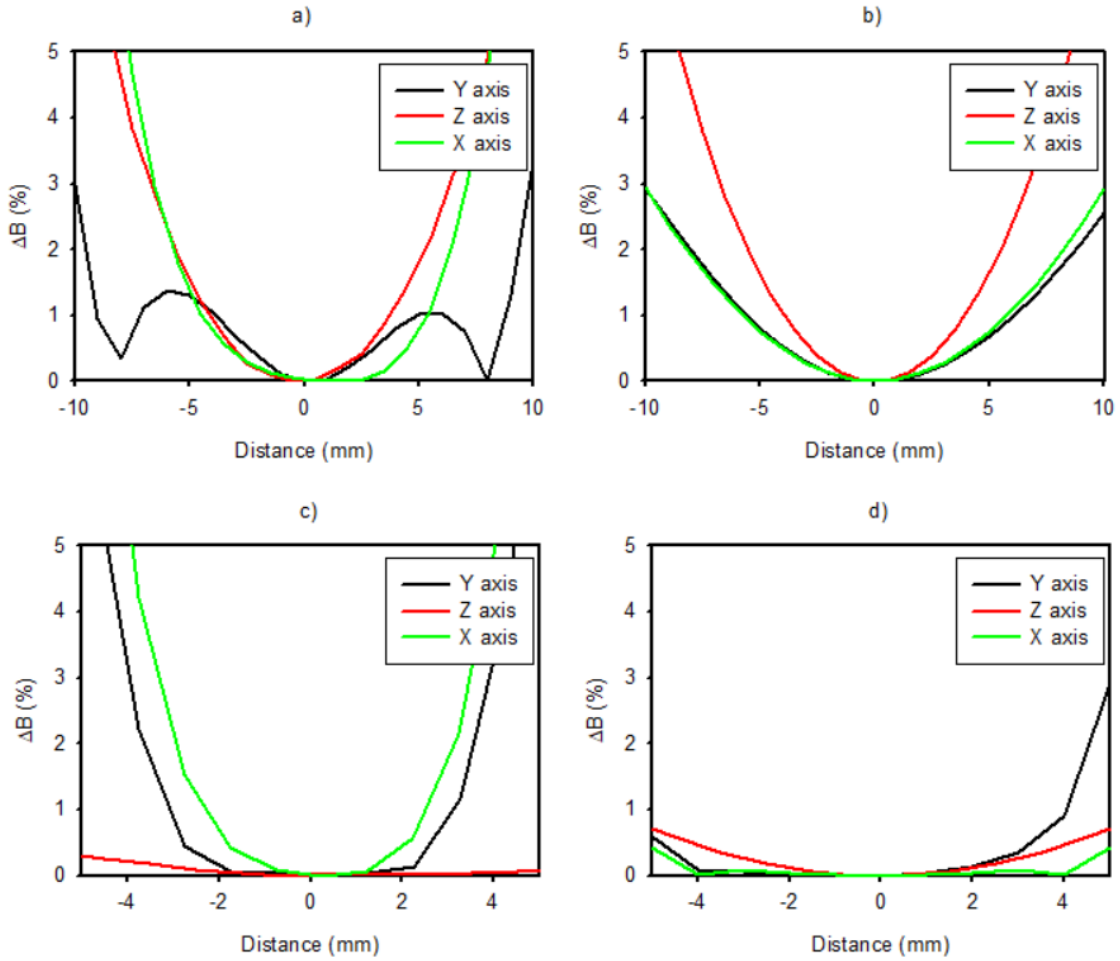

Figure 17. Profiles for B1 field deviation in %. a) saddle coil with 30 mm diameter, b) solenoid coil with 30mm diameter, c) saddle coil with 15 mm diameter and d) solenoid coil with 15 mm diameter.

Finally, being 15 mm the worst case considered for the available gap between the X gradient coils -taking into account the real fabrication possibilities for the gradient coils-, we have simulated once again two different smaller sizes of both topologies, saddle and solenoid coil, one with 10 mm diameter and the other with 12 mm. This time we have taken into account that proximity of the gradient coils to the RF coils would affect the exact B1 distribution and required tuning and matching capacitance, and solenoid has been simulated using copper strip instead of copper wire, in order to be better suited for 3D printed. Figure 18 shows that the 10 mm diameter solenoid will have lower effects from the gradient coils, which are assumed to have a separation of 15 mm for these simulations.

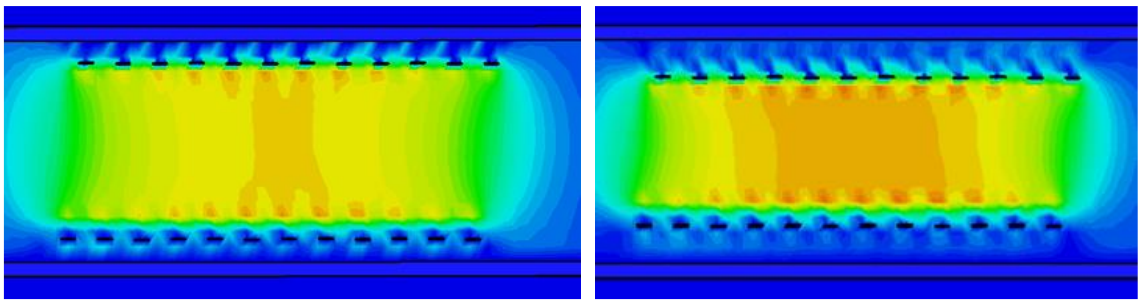

Figure 18: B1 distributions from two different sizes of solenoid coil with different distances from the planar gradient coils. (Left) 12 mm diameter solenoid with 1.5 mm gap on each side to the gradient coil, and (right) 10 mm diameter solenoid with 2.5 mm gap on each side to the gradient coil.

Figure 19 shows the same type of comparison for two saddle coils with diameters 12 mm and 10 mm, respectively.

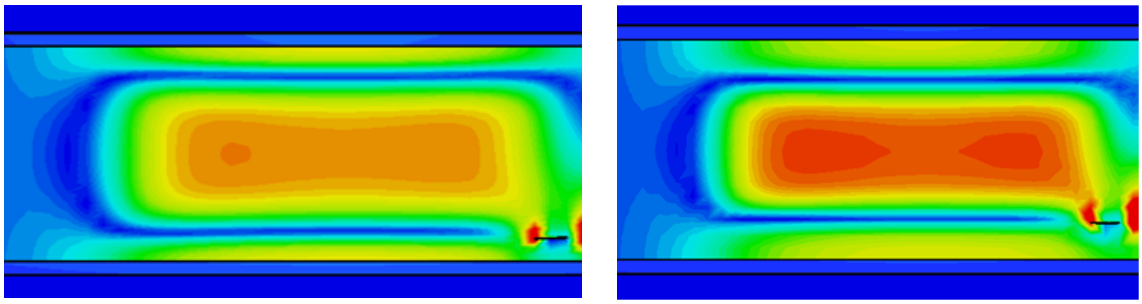

Figure 19: B1 distributions from two different sizes of saddle coil with different distances from the planar gradient coils. (Left) 12 mm diameter saddle with 1.5 mm gap on each side to the gradient coil, and (right) 10 mm diameter saddle with 2.5 mm gap on each side to the gradient coil.

In order to end this section, results shown in Table 3 and Figure 13 may suggest that a solenoid coil is more desirable for this system. However, we prefer not to discard the saddle coil topology since it offers some advantages respect to the solenoid one: eddy currents on a thin segmented structure may be less than on a wound solenoid; electric field at the centre of the solenoid is much greater than that of a saddle coil; and the saddle coil is better suited for 3D printing than solenoid. Thus, as it was mentioned at the beginning, both topologies will be fabricated and tested in the final system in order to find the best behaviour.